

Controlled Agentic Planning & Reasoning for Mechanism Synthesis

João Pedro Gandarela^{1,2} Thiago Rios³ Stefan Menzel³ André Freitas^{1,4,5}

¹Idiap Research Institute, Switzerland

²École Polytechnique Fédérale de Lausanne (EPFL), Switzerland

³Honda Research Institute Europe, Germany

⁴Department of Computer Science, University of Manchester, UK

⁵National Biomarker Centre, CRUK-MI, University of Manchester, UK

firstname.lastname@idiap.ch, joao.gandarela.souza@epfl.ch

firstname.lastname@honda-ri.de, andre.freitas@manchester.ac.uk

Abstract

This work presents a dual-agent Large Language Model (LLM)-based reasoning method for mechanism synthesis, capable of reasoning at both linguistic and symbolic levels to generate geometrical and dynamic outcomes. The model consists of a composition of well-defined functions that, starting from a natural language specification, references abstract properties through supporting equations, generates and parametrizes simulation code, and elicits feedback anchor points using symbolic regression and distance functions. This process closes an actionable refinement loop at the linguistic and symbolic layers. The approach is shown to be both effective and convergent in the context of planar mechanisms. Additionally, we introduce MSynth, a novel benchmark for planar mechanism synthesis, and perform a comprehensive analysis of the impact of the model components. We further demonstrate that symbolic regression prompts unlock mechanistic insights only when applied to sufficiently large architectures.

1 Introduction

The combination of Large Language Model (LLM)-based reasoning with simulation environments (Fu et al., 2024; Bhat et al., 2024; Ichter et al., 2023) represents a promising research stream for systematizing and scaling-up quantitative analysis across areas such as Physics, systems biology and engineering. By interfacing linguistic/symbolic-level interpreters with simulation models, one can develop closed-loop systems where design hypotheses are continuously validated and refined based on dynamic feedback from simulation outputs (Wang et al., 2024; Rana et al., 2023).

The design and synthesis of planar mechanisms is an example of a problem space which requires the coordination of expert-level reasoning steps across different representational domains: language-based, topological, equational, dynamic

and geometric. Traditionally, engineers synthesize mechanisms by using kinematic diagram representations and topological graph-based methods, which provide structured search spaces for the application of conventional optimization algorithms (García-Marina et al., 2020). Typically, the design of a mechanism is divided into two main phases: A conceptual phase and a dimensional synthesis phase (Fig. 1). In the conceptual phase, one defines the overall layout of the mechanism (number of links, number of joints and types of joints) based on the design requirements, e.g., the number of degrees of freedom (Tsai, 1999). Once the layout is fixed, in the dimensional synthesis phase, one defines geometric properties of the links and joints to enable the mechanism to perform a predefined task, which is typically to move the end effector through a predefined trajectory while sustaining mechanical loads (Romero et al., 2019). However, currently available methods for both conceptual design and dimensional synthesis require experienced users, e.g., to select a solution from a set of enumerated conceptual designs, identify redundancies and overconstrained kinematic chains, as well as lack scalability with respect to the complexity of the end effector trajectory and target number of degrees of freedom.

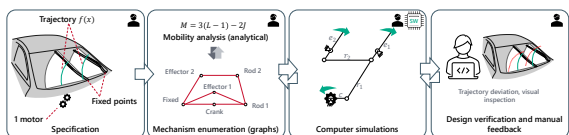


Figure 1: Example of a typical mechanism synthesis workflow of a wind shield wiper mechanism. Engineers initially generate potential solutions as graph representations, which are used as basis for kinematics simulation models in a dimensional synthesis step. Based on the performance of the system in the simulation, the engineers manually and iteratively adjust the system (topology and sizes) until the target performance is achieved.

Recent advancements in machine learning

(Vasiliu and Yannou, 2001; Sonntag et al., 2024), particularly LLMs, have inspired new directions in automated mechanism design. It has been shown that LLMs perform an initial level of linguistic interpretation, simulation code generation/parametrization, thus making them potentially well-suited for addressing the basic reasoning required for mechanism synthesis. However, the reasoning mechanisms for supporting this synthesis remain largely informal, thus limiting the complexity and control of generated mechanisms. The main modelling challenge behind mechanism synthesis lies in the need to reason over and interpret non-linguistic data, e.g. trajectories, geometrical/dynamical properties together with natural language, code generation and equational/mathematical reasoning.

This paper addresses this gap by providing the first end-to-end, well-formalized, cyclic refinement paradigm for mechanism synthesis reasoning. At the center of the proposed model is the decomposition of the formal components involved in the underlying mechanism synthesis reasoning process. The proposed framework is conceptualized across two functional clusters: a Designer Agent ($\mathbb{D}a$) and a Critique Agent ($\mathbb{C}a$) function. While $\mathbb{D}a$ encapsulates the requirements interpretation, mechanism abstraction, mathematical framing, simulation generation and refinement of mechanism configurations, $\mathbb{C}a$ provides a systematic mechanism to evaluate the generated mechanisms based on simulation outcomes, compliance to mechanical constraints and target properties. The iterative dialogue between these two agents creates a constructive feedback loop, wherein systematic design updates and targeted critique drive the convergence towards a mechanism that closely satisfies the specified target properties. These underlying functions, integrate the heterogeneous domains required to perform mechanistic reasoning.

In summary, our contributions are:

1.We propose a mechanism synthesis reasoning framework (design-critique) that integrates LLM-driven design generation with simulation-based evaluation, critique and refinement. **2.**We formalize the underlying systematic design-critique reasoning process, defining an iterative refinement model which, given a set of mechanism requirements, can abstract, instantiate and refine over the mechanism states and properties. **3.**We demonstrate an efficient iterative optimization strategy that leverages a memory repository to capture and build upon

successful design strategies across iterations, ultimately minimizing the deviation between the target and generated trajectories. **4.**We introduce *MSynth*¹ a new benchmark for planar mechanism synthesis. **5.**We empirically analyse the impact of each reasoning component and contrast how different foundation LLM architectures compare in terms of design quality, convergence speed, and computational cost.

The remainder of the paper is organized as follows. Section 2 describes and formalizes the components of the design-critique model. In Section 3, we provide a detailed empirical analysis of the proposed framework. In Section 4, we review methods in mechanism design automation, and finally, Section 5 summarizes our findings and outlines potential directions for future work.

2 Method

In many cases of planar mechanism design, the goal is to generate a mechanism $Mech$ that moves an end effector through a target path, which is described as a set of points or an analytical curve. Given a set of analytical equations \mathcal{T} defining the desired trajectory, our system automatically generates a mechanism configuration that yields a motion path \mathcal{G} that minimizes the deviation with respect to the targeted trajectory and satisfies other design constraints (e.g., number of links).

During the design process, currently available design approaches typically represent mechanisms using graphs and analytical kinematics models. While these representations provide structured search spaces that enable traditional optimization algorithms to explore candidate designs, they require an expert-driven manual set-up and post-hoc analysis (Figure 1). In contrast, we propose an LLM-based reasoning paradigm which, starting from a natural language specification of the requirements, employs a code-based representation to directly specify mechanism components, connections, and parameters. This approach offers greater expressiveness in mechanism specification and yields a broader search space when compared to standard representations. To navigate the design space effectively, at the design phase, we leverage LLMs for supporting an abstract mechanistic reasoning over the mechanism requirements, interpreting mechanics background knowledge, and formalizing a design hypothesis via code genera-

¹anonymized

tion for a target simulator. Within the planar setting, the target mechanism entails a trajectory in the \mathbb{R}^2 domain. Formally, let π_θ denote a pre-trained LLM with parameters θ . We iteratively sample mechanism designs $\mathcal{F} = \text{Mech} : \text{Mech} \sim \pi_\theta$, aiming to minimize the distance d between the target and generated trajectories:

$$\text{Mech*} = \arg \min_{\mathcal{M} \in \text{Mech}} d(\mathcal{T}, \mathcal{G}_{\mathcal{M}})$$

In order to optimize Mech* , the proposed model formalizes an iterative refinement workflow consisting of a Designer Agent ($\mathbb{D}a$), which generates and refines candidate mechanisms, and a Critique Agent ($\mathbb{C}a$), which evaluates the generated designs based on predefined constraints, simulation results, and historical performance data. The agents operate in a feedback loop, where the $\mathbb{C}a$'s evaluations guide the design refinements performed by the $\mathbb{D}a$. Hence, by leveraging both current performance metrics and inferred properties from past iterations, the feedback loop enables the continuous improvement of the designs, which potentially converge to optimal solutions. The following sections describe and formalize the underlying reasoning components that support this adaptive design process (Fig. 2). The overall procedure is formalized in Algorithm 1, which outlines the dual-agent loop of design generation, simulation, critique evaluation, and revision. The proposed model is packaged within *Mechanic*², an adaptative solver for mechanism synthesis.

2.1 Designer Agent

The $\mathbb{D}a$ concentrates the set of functions for the generation of the mechanism design. Given a mechanism specification $\mathcal{M}(\theta)$, Simulator $\mathcal{S}im$, Set of examples $\mathcal{E}x$, Target points along the end effector trajectory \mathcal{P} , and Analytical equation of the target path \mathcal{T} (to provide a closed-form objective against which deviations are measured), the $\mathbb{D}a$ applies an evaluation function:

$$\mathbb{D}a(\mathcal{M}(\theta), \mathcal{S}im, \mathcal{E}x, \mathcal{P}, \mathcal{T}) \rightarrow \text{Mech}$$

Here, the $\mathbb{D}a$ moves from a natural-language description of the task (the prompt and symbolic specs) to a mechanical hypothesis Mech , the instantiation of a mechanism under a simulator $\mathcal{S}im$ that satisfies $\mathcal{M}(\theta)$, and ultimately targets a geometric trajectory in Cartesian (\mathbb{R}^2) space. At each

iteration t (to explore the search space efficiently while maintaining diversity), we sample a batch of b mechanism configurations $F_t = \{f_i\}_{i=1}^b$, $f_i \sim \mathbb{D}a(\cdot \mid p_t)$, where p_t is the constructed prompt (Appendix E). Each candidate is validated via simulation in $\mathcal{S}im$, and those yielding errors are discarded to prevent ill-defined features from propagating into subsequent design iterations. Thus the $\mathbb{D}a$ goes from: linguistic prompt \rightarrow mechanical candidate \rightarrow geometric/ $\mathbb{C}a$ validation \rightarrow refined prompt.

We structure the prompt in four abstraction stages, each adding a layer of guided inference control. First, a motion-profile alignment with the target analytical equations ensure the geometric trajectory faithfully follows the analytic specification. Next, an enforcement of structural constraints, such as naming the critical joint “target”, to guarantee mechanical integrity and facilitate downstream parsing. Then, a systematic refinement via iterative feedback loops that embed linguistic guidance into each design iteration. Finally, a sequential code generation that preserves a clear, logical progression from prompt to executable model. These principles are materialized in a structured prompt composition, formalized as follows (see Appendix F for the complete instantiation):

We now formalize how the $\mathbb{D}a$ integrates these abstractions. Each f_i injects a new reasoning layer:

$$\mathcal{P}_d = f_{\text{Mem}} \circ f_{\text{Con}} \circ f_{\text{Ex}} \circ f_{\text{Sim}}(\text{Input}),$$

where each function f_i represents a distinct processing stage: f_{Sim} : Embeds Simulator documentation and mechanism descriptions; f_{Ex} : Contains concrete examples and reference models; f_{Mem} : Integrates memory containing previous designs and evaluations; f_{Con} : Applies key constraints (key points) and target analytical equations.

The $\mathbb{D}a$ minimizes the deviation (this is the geometric objective that closes the loop back to the analytic target \mathcal{T}) from the target path defined by the function \mathcal{T} . The optimization objective can be formalized as $\arg \min_i d(\mathcal{M}(\theta_i), \mathcal{T})$, where $d(\cdot, \cdot)$ represents a distance metric measuring the deviation from the target \mathcal{T} to the target path $\mathcal{M}(\theta_i)$ at time step i . The $\mathbb{D}a$ iteratively refines the mechanism parameters θ through feedback-driven updates and leverages Symbolic Regression (SR) (Schmidt and Lipson, 2009; Petersen et al., 2021; Shojaee et al., 2025, 2023; Meidani et al., 2024) to extract expressions that guide the optimization.

²anonymized

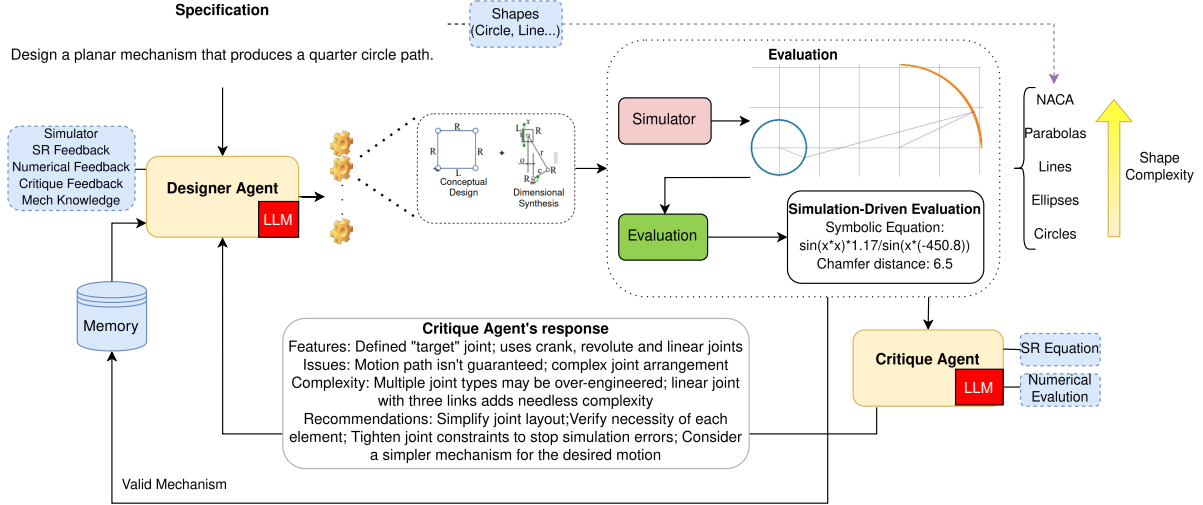


Figure 2: Schematic representation of the proposed LLM-guided design framework for synthesizing planar mechanisms with a quarter-circle end-effector path. A \mathbb{D}_a , guided by domain knowledge and past designs stored in memory, generates mechanism proposals. These proposals are then evaluated using simulation-driven analyses to produce numerical metrics and a Symbolic Regression (SR) equation of the trajectory. The \mathbb{C}_a then assesses the mechanism providing targeted recommendations. Feedback from the simulator and critique loops back to the \mathbb{D}_a to refine subsequent iterations until a valid mechanism is obtained.

2.2 Critique Agent

This agent evaluates designs generated by the \mathbb{D}_a across multiple dimensions and synthesizes structured feedback to guide the iterative design refinement. Given a designed mechanism $\mathcal{M}(\theta)$, Simulator Output \mathcal{S} , Memory repository \mathcal{M}_{mem} , and Designer Response \mathcal{R} (to ground its critique in past designs, fresh simulation data, and the designer’s own rationale), the \mathbb{C}_a applies an evaluation function:

$$\mathbb{C}_a(\mathcal{M}(\theta), \mathcal{S}, \mathcal{M}_{\text{mem}}, \mathcal{R}) \rightarrow \mathbb{F}$$

Here the \mathbb{C}_a maps the geometric output of the simulator back into a linguistic analysis space, producing feedback \mathbb{F} that will inform the next iteration of mechanism hypotheses. The \mathbb{C}_a assessment incorporates specialized knowledge on mechanical design principles and constraints, kinematics simulation and performance analysis (so that feedback reflects not just form but function), historical context based on previous successful designs, structural complexity and optimization potential (Appendix F). Together, these layers abstract and contextualize the numerical simulation output, to inform the next design cycle.

We decompose the \mathbb{D}_a into four abstraction functions, each mapping to properties of the current design state back into linguistic guidance: (1) **Correctness Assessment**: Adherence to constraints and functionality. (2) **Error Identification**: Struc-

tural or functional issues; (3) **Complexity Analysis**: Structural efficiency and design elegance. (4) **Refinement Suggestions**: Actionable design improvements.

We now formalize the \mathbb{C}_a ’s reasoning pipeline, showing how it reconstructs the design story from multiple abstraction layers (Appendix F):

$$\mathcal{P}_c = f_{\text{mem}} \circ f_{\text{sim}} \circ f_{\text{ex}} \circ f_{\text{des}}(I),$$

where each function represents a distinct processing stage: f_{des} : ingests the linguistic output of \mathbb{D}_a as raw critique material. f_{sim} : aligns feedback with fresh geometric/mathematical (SR)/simulation data. f_{ex} : draws on exemplar critiques to standardize style and depth. f_{mem} : grounds each evaluation in historical context for consistency.

2.3 Revision

The revision function operates as a feedback-mediated transformation system that enables iterative refinement of planar mechanisms. Given a Designer Response \mathcal{D}_r , Critique Response \mathcal{C}_r , a Simulator Output \mathcal{S} , and a Memory Repository \mathcal{M}_{mem} , the revision process applies a transformation function:

$$\mathbb{R}_p(\mathcal{D}_r, \mathcal{C}_r, \mathcal{S}, \mathcal{M}_{\text{mem}}) \rightarrow \mathcal{D}'_r$$

Here the revision function bridges from the linguistic artifacts of designer and critic back into

a mechanical proposal (\mathcal{D}'_r), ready for geometric validation in the next loop.

where: \mathbb{R}_p : Revision function responsible for mechanism refinement; \mathcal{D}_r : Designer Response containing the current mechanism implementation; \mathcal{C}_r : Critique Response providing structured feedback; \mathcal{S} : Simulator Output containing execution traces and validation results; $\mathcal{M}em$: Memory Repository storing previous designs and outcomes; \mathcal{D}'_r : Refined Designer Response with improved implementation.

At each refinement iteration t , we generate a revised mechanism $\mathcal{D}'_{r,t}$ based on the previous implementation and feedback:

$$\mathcal{D}'_{r,t} = \mathbb{R}_p(\mathcal{D}_{r,t-1}, \mathcal{C}_{r,t-1}, \mathcal{S}_{t-1}, \mathcal{M}em_{t-1})$$

This iterative rule encapsulates how the system cycles through linguistic feedback, mechanical transformation, and geometric re-evaluation.

We codify three constraint checks, each ensuring the revision stays true to its linguistic instructions, mechanical fidelity, and geometric performance:

Feedback Adherence: The revision incorporates and addresses the provided critique:

$$\forall f \in \mathcal{C}_{r,t-1}, \exists m \in \mathcal{D}'_{r,t} : \text{Addresses}(m, f) = 1$$

Simulation Consistency: The revised mechanism aligns with physical simulation principles:

$$\mathcal{V}(\mathcal{M}(\theta)'_{r,t}, \mathcal{S}_{t-1}) = 1$$

Efficiency: The revision eliminates redundancy while maintaining functional correctness:

$$\text{Complexity}(\mathcal{M}(\theta)'_{r,t}) \leq \text{Complexity}(\mathcal{M}(\theta)_{r,t-1})$$

subject to $d(\mathcal{D}'_{r,t}, \mathcal{T}) \leq d(\mathcal{D}_{r,t-1}, \mathcal{T})$.

We materialize the revision function's prompt, layering linguistic inputs through mechanical checks and geometric validation (Appendix G):

$$\mathcal{P}_r = f_{\text{mem}} \circ f_{\text{sim}} \circ f_{\text{crit}} \circ f_{\text{des}}(\text{Input})$$

where each function represents a distinct processing stage. The first, f_{des} , incorporates the current $\mathbb{D}a$ Response (to re-ingest the designer's latest implementation as the starting point). Next, f_{crit} applies structured critique from the $\mathbb{C}a$ (to inject targeted, linguistic feedback into the revision prompt). Then, f_{sim} integrates empirical validation via simulation outcomes (to align proposed changes with up-to-date geometric/SR simulation results). Finally, f_{mem} leverages historical context from successful past designs (to recall proven patterns and avoid repeating mistakes).

The ultimate objective of the revision function is to minimize the discrepancy between the target trajectory and the mechanism-generated path. The process terminates when either the distance falls below an acceptable threshold ϵ or the maximum number of revision iterations R_{\max} is reached: $d(\mathcal{M}(\theta)'_{r,t}, \mathcal{T}) \leq \epsilon$ or $t \geq R_{\max}$

2.4 Memory

The optimization framework incorporates a memory system that captures and leverages previously validated mechanisms. In the optimization process, the memory represents a structured repository of previously validated mechanisms. Formally: Let $M_t = \{m_1, m_2, \dots, m_n\}$ denote the set of stored mechanisms at iteration t . A mechanism m_i is stored only if it satisfies the execution criterion:

$$\mathcal{V}(m_i) = 1, \quad \text{where } \mathcal{V}(m_i) \text{ is a validity function.}$$

Retrieval follows a selection function:

$$m_{\text{retrieved}} = \arg \min_{m_i \in M_t} d(m_i, m_{\text{target}}),$$

where $d(\cdot, \cdot)$ represents a predefined distance metric.

Memory within this framework consists exclusively of mechanisms that executed successfully in the simulation environment. This selective storage approach ensures the validity preservation across the mechanism repository, improves the computational efficiency through elimination of invalid designs, and favours the convergence of the design refinement via retention of proven designs. The storage increases proportionally with iterations, creating a progressively richer knowledge base that guides subsequent iterations.

Retrieval Methodology. The memory retrieval implements a proximity-based selection strategy:

1. Retrieval Criterion: Mechanisms are prioritized based on their closeness to the current design objectives and *2. Multi-Exemplar Scenario:* When multiple examples are needed, the system retrieves the top- k mechanisms with the smallest distances, where k corresponds to the number of requested examples. Through the alignment of retrieved designs with current objectives, the memory component facilitates the transfer of successful principles from past iterations to new designs, by continuously adapting and leveraging experience throughout the optimization process.

3 Empirical Analysis

In this section, we present an empirical analysis to evaluate the mechanistic synthesis framework in an automated planar mechanism design scenario. The study aims to address the following research questions: **RQ1:** How does cyclic refinement affect the depth and precision of the search process in automated mechanism synthesis? **RQ2:** In what ways do symbolic representation features modulate the exploration-exploitation trade-off during design iteration? **RQ3:** How do different foundation LLM architectures compare in terms of design quality, convergence speed, and computational cost? **RQ4:** What are the distinct contributions of individual system components (e.g., memory, $\mathbb{C}a$) to overall performance? **RQ5:** To what extent does integrating mechanistic knowledge accelerate systematic exploration and improve solution quality when employing large-scale LLMs?

Experimental Setup. To support the evaluation, we build a synthetic dataset which evaluates mechanism generation across a set of trajectories which are analytically defined, including elliptical, lemniscate, and complex polynomial paths, parametrized by increasing geometric complexity (the set of analytical shapes are defined in Appendix C). In our experiments, each iteration samples 3 mechanisms from $\mathbb{D}a$ with temperature 0.8. These settings are designed to stress-test the dual-agent loop under controlled conditions. We set the $R_{max} = 20$ and $\epsilon = 0.05$, used the PyLinkage simulation framework (Farajallah, 2024) to compute the trajectory of the end effector and PySR to compute the Symbolic Regression (SR) feedback (Cranmer, 2023). Finally, we applied the Iterative Closest Point (ICP) algorithm, using the implementation by (Drakoulis, 2023; Lu and Milios, 1997), to align the simulated and measured point clouds and thus refine the end-effector pose. The overall performance of the system is quantified based on both the Chamfer distance ($d_{Chamfer}$) for geometric fidelity and the number of iterations (t_{iter}) for efficiency.

Interventions. We compare the impact of each functional component: memory retrieval (enabled vs. disabled), $\mathbb{C}a$ feedback (full vs. none), and large language models (Llama3:70B (Llama3:70B) (AI@Meta, 2024; Grattafiori et al., 2024), Gemma3:12B (Gemma3:12B) (Team, 2025a), Qwen:4B (Qwen:4B) (Team, 2025b)) to isolate their individual effects. Our workflow, sum-

marized in Algorithm 1, mirrors the dual-agent optimization cycle: Designer Sampling of b candidate mechanisms by $\mathbb{D}a$, Simulation Validation to filter invalid designs, Critique Evaluation via $\mathbb{C}a$ for correctness and refinement potential, Revision to generate $\mathcal{D}'r$, and Termination when $d_{Chamfer} \leq \epsilon$ or the iteration limit R_{max} is reached. By systematically varying one factor at a time, we isolate the contribution of each component and obtain quantitative comparisons across different experimental conditions.

Dataset. We evaluate our approach on a set \mathcal{S} of target trajectories based on six analytic planar curves: circles, ellipses, lines, parabolas, Lemniscates of Bernoulli (∞) (LB), and NACA four-digit airfoils (Jacobs et al., 1933; Abbott and Von Doenhoff, 2012), each parameterized by standard formulae. By measuring mean Chamfer distance, we observe a progression of trajectories of increasing complexity: LB (easiest), then circles, ellipses, lines, parabolas, and finally NACA airfoils (hardest). For each shape class, we generate 5 random instances by sampling shape parameters uniformly over their valid ranges, then draw $n \in \{4\}$ equally-spaced points along the curve to form the target motion profile. More details on the dataset are provided in Appendix C and H.

Evaluation Metrics. Evaluation is performed using a composition of metrics *Chamfer Distance* and *Pass@n*. Trajectories are normalized under *Point Set Alignment*. The metrics are detailed in Appendix B.

3.1 Results

The proposed mechanistic synthesis reasoning model delivers geometric outcomes via a linguistic/symbolic interpretation. Regarding RQ1, the proposed model allows mechanistic synthesis reasoning to be delivered by the systematic composition of linguistic specification, abstraction, simulation code generation, simulator evaluation, and repeated critique-driven refinement. While mechanism synthesis is an essentially dynamical/geometrical problem, it can be steered in a linguistic/symbolic form by the functional decomposition outlined in Sections 2.1, 2.2, and 2.3, which converges towards the desired geometric outcome. Initial iterations explore broad regions (e.g., Gemma3:12B first Chamfer: 7.905 → 6.11; Llama3:70B: 9.8245 → 4.5867); Qwen:4B: 11.17 → 4.965) up to 55.56%. Subsequent feedback-driven cycles exploit local op-

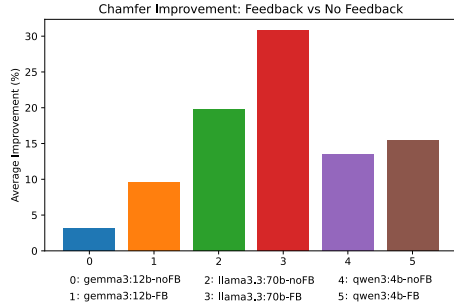


Figure 3: Average percentage improvement in Chamfer distance when comparing runs without feedback (noFB) versus with feedback (FB). Incorporating feedback yields substantial gains, with the largest uplift observed for Llama3:70Bs (from 19% to 29%), demonstrating that feedback consistently enhances performance. The feedback is provided by the $\mathbb{C}a$.

tima, yielding up to 31.3% Chamfer reduction for Gemma3:12B ($8.081 \rightarrow 5.552$) and up to 78.9% for Llama3:70B with combined equations (circle: $13.53 \rightarrow 2.86$). Gemma3:12B converges in $\sim 8.7\text{--}9$ steps, Llama3:70B in $\sim 9.7\text{--}10$ steps, and Qwen:4B in $\sim 8.7\text{--}9$ steps, confirming that cyclic refinement alternates exploration and critique to balance coverage and precision.

Feedback (critique) is the most impactful component across models. Addressing **RQ2**, this demonstrates how transitioning from a purely linguistic prompt to mechanical candidate proposals enriched by critique, and subsequently evaluating them in the simulator, leads to geometric accuracy gains. Enabling feedback alone yields +31.3% Chamfer improvement for Gemma3:12B, +78% for Llama3:70B, and +40.4% for Qwen:4B. Feedback raises Pass@ to 1.0 for Gemma3:12B (from 0.9845), ensures that Llama3:70B reaches flawless reliability without memory, and accelerates iterative refinement across all models, underlining its universal importance. Figure 3 shows that adding $\mathbb{C}a$ feedback boosts final Chamfer gains across all three model families.

Equational prompts affect large-scale models and those trained with chain-of-thought reasoning. Here, we observe the manner in which the in-context injection of SR equations facilitates the subsequent mechanical code proposals and guides the LLM towards the correct mechanism. For Llama3:70B, equation-only prompts cut Chamfer error by 51.2% on circles and 35.1% on ellipses within 5-9 iterations, and Qwen:4B exhibits similar reductions (38.4% circle, 43.7% ellipse). In

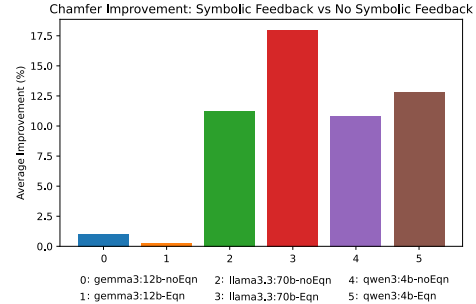


Figure 4: Average percentage improvement in Chamfer distance when comparing runs without SR feedback (noEqn) versus with SR feedback (Eqn). Incorporating SR feedback yields gains for the Qwen:4B and large-scale models, most notably boosting Llama3:70B from 11% to 17% and Qwen:4B from 10% to 13%, while the Gemma3:12B model sees minimal change. These results demonstrate that SR feedback can significantly enhance performance.

Model	#Param	Chamfer Gain (Vanilla)	Mean Imp %	Best Steps
Qwen	4B	up to 55.5%	16.9	~ 8.7
Gemma	12B	up to 31.4%	7.9	~ 9.2
Llama	70B	up to 55.1%	30.0	~ 9.8

Table 1: Comparison of across different base models.

contrast, Gemma3:12B shows no systematic improvement, averaging a Chamfer of 1.046% without the SR equation prompts versus 0.25% when given SR feedback, indicating that only sufficiently large or chain-of-thought trained models can harness symbolic scaffolds for meaningful gains. Figure 4 shows that adding SR feedback boosts the final Chamfer gains on large LLMs or trained with chain-of-thought reasoning.

Architectural scale plays a significant role in design quality. In response to **RQ3**, we refer to Table 1, architectural differences strongly influence the reduction in Chamfer distance. Gemma3:12B delivers up to 31.4% Chamfer gains, Llama3:70B achieves up to 55.1%, and Qwen:4B balances up to 55.5% gains. Moreover, while Qwen:4B forgoes expert routing, its dense model still performs multi-step internal reasoning. This enables the model to interpret mechanistic prompts and deliver moderate Chamfer gains up to 55.1%, comparable to Llama3:70B without specialized attention mechanisms. Larger models inherently explore more thoroughly, while smaller models trade resource demands for adaptability.

Memory exhibit model-specific effects. With respect to **RQ4**, when running Gemma3:12B,

mem=2 without feedback worsens Chamfer (6.11→9.01) and drops Pass@ (0.9845→0.9531). Even with feedback, memory reduces Chamfer gains from 31.3% to 21.7%. Conversely, Llama3:70B’s mem=2 adds only a 3.5% gain but ensures Pass@=1.0, while Qwen:4B shows outcomes of up to +46.97%, indicating memory’s trade-off between noise and redundancy varies by architecture.

Two exemplars optimize convergence efficiency. Concerning **RQ5**, two-shot prompting ($n=2$) defines an optimal feedback point. For Gemma3:12B on “LB”: $n=2 \rightarrow 6.11$ vs. $n=3 \rightarrow 7.991$; with feedback: $n=2 \rightarrow 5.552$ in 8.25 steps vs. $n=3 \rightarrow 5.917$ in 10.75 steps. Llama3:70B and Qwen:4B exhibit similar trends, confirming that minimal exemplars drive rapid, high-quality refinement.

4 Related Work

Neuro Symbolic and Reasoning LLMs show promise in formal reasoning, yet struggle to compose complex structures, motivating self-refinement techniques that loop model outputs back as feedback (Dziri et al., 2023; Madaan et al., 2023; Huang and Chang, 2023). Systems coupling dynamic geometry kernels with automated theorem provers let users symbolically verify linkage invariants in real time (Recio and Vélez, 2020). Our proposed model sophisticates this reasoning function : the design agent generates simulator code, and the critique agent provides an actionable feedback via SR outputs and distance metrics to bridge symbolic reasoning and numeric optimization.

Agentic Coordination and Execution LLMs can decompose complex tasks into subgoals but often lack dynamic subgoal allocation and real-time state feedback (Xiang et al., 2024); hierarchical planner-executor-reviewer loops interleave symbolic plan generation with concrete API/simulator calls (Shang et al., 2025) and incorporate reinforcement-style critique for optimized performance (Yang et al., 2025; Hu et al., 2024), bridging symbolic reasoning and numeric optimization (Wu et al., 2024; Gürler et al., 2021).

Deep Generative Models for Mechanism Synthesis Conditional GANs for crank-rocker four-bar linkages learn the mapping from target coupler trajectories to linkage parameters, outperforming NSGA-II and cVAE in both speed and solution diversity by avoiding costly fitness evaluations (Bai

and Angeles, 2015; Lee et al., 2024). Unlike these one-shot neural generators, our design agent integrates SR, $\mathbb{C}a$, and simulator feedback in a loop to iteratively refine parameters, in an explicit step-wise reasoning setting.

Optimization-Based Linkage Design Gradient-based frameworks like MaGI optimize motion synthesis over topologies and dimensions but hinge on good initial guesses and penalty weights for convergence (Singh et al., 2024). Instead this work embeds an LLM-mediated controller that fuses distances with SR insights to produce interpretable, data-driven parameter updates.

Data-Driven Kinematic Design LINKS provides a vast search space of over 100 million 1-DOF linkages and 1.1 billion coupler curves via rapid topology operators and vectorized simulation (nob, 2022; Nobari et al., 2024), and the ASME dataset adds 3 million four-, six-, and eight-bar mechanisms benchmarked on standard kinematic metrics (Nurizada et al., 2025; Venkataraman et al., 2018; Martín-Martín et al., 2018). In contrast, our dual-agent pipeline dynamically generates and critiques mechanisms, rather than querying a fixed database, to iteratively refine designs toward arbitrary analytical curves.

5 Conclusion

In this work, we introduced a dual-agent LLM-based reasoning method for mechanism synthesis, which reasons at a linguistic/symbolic level to deliver geometrical and dynamic outcomes. The proposed model provides a composition of well-defined functions which, starting from a NL specification, refers to abstract properties via supporting equations, generates and parametrizes a simulation code, elicits feedback anchor points using symbolic regression and distance functions, closing an actionable refinement loop at a linguistic/symbolic layer. The proposed approach showed to be effective and convergent in the context of planar mechanisms. We further introduced MSynth, a new benchmark for planar mechanism synthesis. Through comprehensive ablations, we establish the $\mathbb{C}a$ ’s *feedback* as the single most transformative component, yielding up to a 78% reduction in Chamfer distance. We further show that symbolic regression prompts unlock mechanistic insights only in sufficiently large architectures.

6 Limitations

While the proposed method demonstrated strong empirical gains across all models further investigation is required on addressing the causal factors on the differences of performance across different models. Despite the fact that all LLMs exhibited chamfer gains, their underlying LLM characteristics, particularly their model size and training regimen (e.g. Qwen’s step-by-step reasoning training prior to producing its final answer), plays a role. Large-capacity LLMs (Llama) effectively exploit symbolic equation prompts, whereas smaller models (Gemma) deliver more timid results. Finally, our experiments focus exclusively on fitting 2D geometric primitives (lines, circles, ellipses, parabolas, NACA airfoils), leaving its effectiveness in high-dimensional design spaces still as a future objective.

7 Ethical Statement

This work explores AI-driven mechanisms to automate the systematic design of mechanism synthesis. While the work demonstrates this as a promising research direction, the proposed method is exploratory and should not be applied at this stage as a substitute to manual engineering design. Further investigation is required to critically understand the limitations of the proposed method when dialoguing with more complex mechanism synthesis scenarios.

8 Acknowledgements

This work was funded by the Honda Research Institute Europe GmbH (HRI) through the Mechanic project.

References

2022. *LINKS: A Dataset of a Hundred Million Planar Linkage Mechanisms for Data-Driven Kinematic Design*, volume Volume 3A: 48th Design Automation Conference (DAC) of International Design Engineering Technical Conferences and Computers and Information in Engineering Conference. V03AT03A013.

Ira H Abbott and Albert E Von Doenhoff. 2012. *Theory of wing sections: including a summary of airfoil data*. Courier Corporation.

AI@Meta. 2024. [Llama 3 model card](#).

Shaoping Bai and Jorge Angeles. 2015. *Coupler-curve synthesis of four-bar linkages via a novel formulation*. *Mechanism and Machine Theory*, 94:177–187.

Vineet Bhat, Ali Umut Kaypak, Prashanth Krishnamurthy, Ramesh Karri, and Farshad Khorrami. 2024. [Grounding llms for robot task planning using closed-loop state feedback](#). *Preprint*, arXiv:2402.08546.

Mark Chen, Jerry Tworek, Heewoo Jun, Qiming Yuan, Henrique Ponde de Oliveira Pinto, Jared Kaplan, Harri Edwards, Yuri Burda, Nicholas Joseph, Greg Brockman, Alex Ray, Raul Puri, Gretchen Krueger, Michael Petrov, Heidy Khlaaf, Girish Sastry, Pamela Mishkin, Brooke Chan, Scott Gray, and 39 others. 2021. [Evaluating large language models trained on code](#). *Preprint*, arXiv:2107.03374.

Miles Cranmer. 2023. [Interpretable machine learning for science with pysr and symbolicregression.jl](#). *Preprint*, arXiv:2305.01582. This work is licensed under the Apache-2.0 license <https://github.com/MilesCranmer/PySR/blob/master/LICENSE>.

Richardos Drakoulis. 2023. [Iterative closest point](#). <https://github.com/richardos/icp>. Accessed: 2025-05-19.

Nouha Dziri, Ximing Lu, Melanie Sclar, Xiang Lorraine Li, Liwei Jiang, Bill Yuchen Lin, Sean Welleck, Peter West, Chandra Bhagavatula, Ronan Le Bras, Jena D. Hwang, Soumya Sanyal, Xiang Ren, Allyson Ettinger, Zaid Harchaoui, and Yejin Choi. 2023. [Faith and fate: Limits of transformers on compositionality](#). In *Thirty-seventh Conference on Neural Information Processing Systems*.

Hugo Farajallah. 2024. [pylinkage: Python linkage builder and optimizer](#). <https://github.com/HugoFara/pylinkage>. GitHub repository (v0.6.0, released Oct 2 2024; accessed 2025-05-08); This work is licensed under the MIT License <https://github.com/HugoFara/pylinkage/blob/main/LICENSE>.

Daocheng Fu, Wenjie Lei, Licheng Wen, Pinlong Cai, Song Mao, Min Dou, Botian Shi, and Yu Qiao. 2024. [Limsim++: A closed-loop platform for deploying multimodal llms in autonomous driving](#). *Preprint*, arXiv:2402.01246.

V. García-Marina, I. Fernández de Bustos, G. Urkullu, and R. Ansola. 2020. [Optimum dimensional synthesis of planar mechanisms with geometric constraints](#). *Mecánica*, 55(11):2135–2158.

Aaron Grattafiori, Abhimanyu Dubey, Abhinav Jauhri, Abhinav Pandey, Abhishek Kadian, Ahmad Al-Dahle, Aiesha Letman, Akhil Mathur, Alan Schelten, Alex Vaughan, Amy Yang, Angela Fan, Anirudh Goyal, Anthony Hartshorn, Aobo Yang, Archi Mitra, Archie Sravankumar, Artem Korenev, Arthur Hinsvark, and 542 others. 2024. [The llama 3 herd of models](#). *Preprint*, arXiv:2407.21783.

Nico Görtler, Dieter Büchler, and Georg Martius. 2021. [Hierarchical reinforcement learning with timed subgoals](#). *Advances in Neural Information Processing Systems*, 34.

Mengkang Hu, Tianxing Chen, Qiguang Chen, Yao Mu, Wenqi Shao, and Ping Luo. 2024. **Hiagent: Hierarchical working memory management for solving long-horizon agent tasks with large language model.** *Preprint*, arXiv:2408.09559.

Jie Huang and Kevin Chen-Chuan Chang. 2023. **Towards reasoning in large language models: A survey.** In *Findings of the Association for Computational Linguistics: ACL 2023*, pages 1049–1065, Toronto, Canada. Association for Computational Linguistics.

brian ichter, Anthony Brohan, Yevgen Chebotar, Chelsea Finn, Karol Hausman, Alexander Herzog, Daniel Ho, Julian Ibarz, Alex Irpan, Eric Jang, Ryan Julian, Dmitry Kalashnikov, Sergey Levine, Yao Lu, Carolina Parada, Kanishka Rao, Pierre Sermanet, Alexander T Toshev, Vincent Vanhoucke, and 26 others. 2023. **Do as i can, not as i say: Grounding language in robotic affordances.** In *Proceedings of The 6th Conference on Robot Learning*, volume 205 of *Proceedings of Machine Learning Research*, pages 287–318. PMLR.

E. N. Jacobs, K. E. Ward, and R. M. Pinkerton. 1933. **The characteristics of 78 related airfoil sections from tests in the variable-density wind tunnel.** Technical Report Report No. 460, National Advisory Committee for Aeronautics (NACA).

Sumin Lee, Jihoon Kim, and Namwoo Kang. 2024. Deep generative model-based synthesis of four-bar linkage mechanisms with target conditions. *arXiv preprint arXiv:2402.14882*.

Feng Lu and Evangelos Milios. 1997. Robot pose estimation in unknown environments by matching 2d range scans. *Journal of Intelligent and Robotic systems*, 18:249–275.

Aman Madaan, Niket Tandon, Prakhar Gupta, Skyler Hallinan, Luyu Gao, Sarah Wiegreffe, Uri Alon, Nouha Dziri, Shrimai Prabhumoye, Yiming Yang, Shashank Gupta, Bodhisattwa Prasad Majumder, Katherine Hermann, Sean Welleck, Amir Yazdankhsh, and Peter Clark. 2023. **Self-refine: Iterative refinement with self-feedback.** In *Thirty-seventh Conference on Neural Information Processing Systems*.

Roberto Martín-Martín, Clemens Eppner, and Oliver Brock. 2018. **The rbo dataset of articulated objects and interactions.** *Preprint*, arXiv:1806.06465.

Kazem Meidani, Parshin Shojaee, Chandan K. Reddy, and Amir Barati Farimani. 2024. **SNIP: Bridging mathematical symbolic and numeric realms with unified pre-training.** In *The Twelfth International Conference on Learning Representations*.

Amin Heyrani Nobari, Akash Srivastava, Dan Gutfreund, Kai Xu, and Faez Ahmed. 2024. **Link: Learning joint representations of design and performance spaces through contrastive learning for mechanism synthesis.** *Preprint*, arXiv:2405.20592.

Anar Nurizada, Rohit Dhaipule, Zhijie Lyu, and Anurag Purwar. 2025. A dataset of 3m single-dof planar 4-, 6-, and 8-bar linkage mechanisms with open and closed coupler curves for machine learning-driven path synthesis. *Journal of Mechanical Design*, 147(4).

Brenden K Petersen, Mikel Landajuela, T Nathan Mundhenk, Claudio P Santiago, Soo K Kim, and Joanne T Kim. 2021. Deep symbolic regression: Recovering mathematical expressions from data via risk-seeking policy gradients. In *Proc. of the International Conference on Learning Representations*.

Krishan Rana, Jesse Haviland, Sourav Garg, Jad Abou-Chakra, Ian Reid, and Niko Suenderhauf. 2023. **Say-plan: Grounding large language models using 3d scene graphs for scalable task planning.** In *7th Annual Conference on Robot Learning*.

Zoltán Kovács Tomás Recio and M. Pilar Vélez. 2020. **Reasoning about linkages with dynamic geometry.** *Journal of Symbolic Computation*, 97:16–30. Special issue on dynamic geometry and automated reasoning.

Neider Nadid Romero, Alexandre Campos, Daniel Martins, and Rodrigo S. Vieira. 2019. **A new approach for the optimal synthesis of four-bar path generator linkages.** *SN Applied Sciences*, 1(11):1504.

Michael Schmidt and Hod Lipson. 2009. **Distilling free-form natural laws from experimental data.** *Science*, 324(5923):81–85.

Yu Shang, Yu Li, Keyu Zhao, Likai Ma, Jiahe Liu, Fengli Xu, and Yong Li. 2025. **Agentsquare: Automatic LLM agent search in modular design space.** In *The Thirteenth International Conference on Learning Representations*.

Parshin Shojaee, Kazem Meidani, Amir Barati Farimani, and Chandan K. Reddy. 2023. **Transformer-based planning for symbolic regression.** In *Thirty-seventh Conference on Neural Information Processing Systems*.

Parshin Shojaee, Kazem Meidani, Shashank Gupta, Amir Barati Farimani, and Chandan K. Reddy. 2025. **LLM-SR: Scientific equation discovery via programming with large language models.** In *The Thirteenth International Conference on Learning Representations*.

Ramanpreet Singh, Vimal Kumar Pathak, Ashish Kumar Srivastava, Rakesh Kumar, and Abhishek Sharma. 2024. A new metaphor-less optimization algorithm for synthesis of mechanisms. *International Journal on Interactive Design and Manufacturing (IJIDeM)*, 18(4):2371–2391.

Sebastian Sonntag, Vincent Brünjes, Janosch Luttmer, Burkhard Corves, and Arun Nagarajah. 2024. Machine learning applications for the synthesis of planar mechanisms—a comprehensive methodical literature review. In *International Design Engineering Technical Conferences and Computers and Information in Engineering Conference*, volume 88414, page

V007T07A003. American Society of Mechanical Engineers.

Gemma Team. 2025a. [Gemma 3](#).

Qwen Team. 2025b. [Qwen3](#).

L. W. Tsai. 1999. Systematic enumeration of parallel manipulators. In *Parallel Kinematic Machines*, pages 33–49, London. Springer London.

Adrian Vasiliu and Bernard Yannou. 2001. Dimensional synthesis of planar mechanisms using neural networks: application to path generator linkages. *Mechanism and Machine Theory*, 36(2):299–310.

Abhishek Venkataraman, Brent Griffin, and Jason J. Corso. 2018. [Learning kinematic descriptions using spare: Simulated and physical articulated extendable dataset](#). *Preprint*, arXiv:1803.11147.

Lirui Wang, Yiyang Ling, Zhecheng Yuan, Mohit Shridhar, Chen Bao, Yuzhe Qin, Bailin Wang, Huazhe Xu, and Xiaolong Wang. 2024. [Gensim: Generating robotic simulation tasks via large language models](#). In *The Twelfth International Conference on Learning Representations*.

Yue Wu, Yewen Fan, So Yeon Min, Shrimai Prabhu-moye, Stephen Marcus McAleer, Ruslan Salakhutdinov, Yonatan Bisk, Yuanzhi Li, and Tom Mitchell. 2024. [Agentkit: Structured LLM reasoning with dynamic graphs](#). In *First Conference on Language Modeling*.

Yufei Xiang, Yiqun Shen, Yeqin Zhang, and Nguyen Cam-Tu. 2024. [Retrospecx: Language agent meets offline reinforcement learning critic](#). In *Proceedings of the 2024 Conference on Empirical Methods in Natural Language Processing*, pages 4650–4666, Miami, Florida, USA. Association for Computational Linguistics.

Ke Yang, Yao Liu, Sapana Chaudhary, Rasool Fakoor, Pratik Chaudhari, George Karypis, and Huzeifa Rangwala. 2025. [Agentoccam: A simple yet strong baseline for LLM-based web agents](#). In *The Thirteenth International Conference on Learning Representations*.

A Method Algorithm

In this section, we provide a detailed description of our dual-agent iterative design loop for synthesising planar mechanisms (see Algorithm 1). Starting with an initial set of parameters, the $\mathbb{D}a$ proposes a candidate mechanism, which is then simulated on $\mathcal{S}im$. Successful simulations trigger a distance-metric evaluation against the target trajectory \mathcal{T} , and SR feedback. The validated design is then stored in memory. The $\mathbb{C}a$ then assesses performance and provides feedback on how to refine the design, prompting the $\mathbb{D}a$ to generate updated parameters for a second simulation and re-evaluation. This cycle of design, simulation, evaluation and refinement repeats until the mechanism meets the predefined convergence or performance criteria.

Algorithm 1 Iterative Planar Mechanism Design with Dual Agent, Simulation, and Evaluation

```

1: Input: Initial design parameters, Simulator on  $Sim$ , evaluation functions, target trajectory  $\mathcal{T}$ 
2: Output: Optimized planar mechanism design  $\mathcal{M}(\theta)$ 
3: while Design objective not met do
4:   Design: Generate a new planar mechanism  $\mathcal{M}(\theta)$  using the  $\mathbb{D}a$ .
5:   First Simulation: Simulate  $\mathcal{M}(\theta)$  on  $Sim$ 
6:   if Simulation successful then
7:     Compute distance metric  $d(\mathcal{M}(\theta), \mathcal{T})$ 
8:     Discover SR equation
9:     Store  $\mathcal{M}(\theta)$  in memory
10:  end if
11:  •  $\mathbb{C}a$  evaluates the mechanism and provides feedback
12:  Refinement: Update the design strategy using feedback from the evaluation
13:  Design (Refinement): Generate a refined mechanism  $\mathcal{M}'(\theta)$  using the updated strategy.
14:  Simulation: Simulate the refined mechanism  $\mathcal{M}'(\theta)$  on  $Sim$ 
15:  if Simulation successful then
16:    Store  $\mathcal{M}'(\theta)$  in memory
17:  else
18:    Discard  $\mathcal{M}'(\theta)$ 
19:    continue to the next iteration
20:  end if
21:  Evaluation:
22:  • Re-compute the distance metric  $d(\mathcal{M}'(\theta), \mathcal{T})$ 
23:  • Re-assess SR feedback
24: end while
25: return Best mechanism  $\mathcal{M}(\theta)$  or refined mechanism  $\mathcal{M}'(\theta)$  meeting design criteria

```

B Evaluation Metrics

Point Set Alignment. For a generated mechanism m_t that yields an end effector trajectory $GeneratedPoints$, we first perform point set registration via the ICP algorithm to establish the correspondence with the target motion profile. The algorithm aligns the generated point set with the target point set through rigid transformations, which compensates the differences in the orientation of the coordinate systems.

Chamfer Distance. Following the trajectory alignment, the mechanism’s performance is quantified

using the Chamfer distance metric, which provides a bidirectional measure of spatial proximity between the two point sets.

Pass@. We compute Pass@ (Chen et al., 2021) over the *entire* iterative generation process: each of the k samples is drawn and evaluated, and the metric reflects the probability that *at least one* of those k attempts succeeds. A generated program is considered successful if it meets two correctness criteria: (i) it contains no syntax errors, and (ii) it can be executed without failure by the target simulator. Only programs satisfying both conditions are counted as valid. More details on the evaluation metrics are provided in Appendix D.

C Dataset Details

Let

$$\begin{aligned} \mathcal{S} = \{ & \mathcal{C}(r, x_1, y_1), \\ & \mathcal{E}(a, b, x_1, y_1), \\ & \mathcal{L}(x_1, y_1, x_2, y_2), \\ & \mathcal{P}(a, h, k), \\ & \mathcal{B}(a), \\ & \mathcal{N}(\text{series}) \}, \end{aligned}$$

where $r, a, b > 0$, $(x_1, y_1), (x_2, y_2), (h, k) \in \mathbb{R}^2$, $a \neq 0$, and “series” ranges over the standard NACA four-digit codes $\{2000, \dots, 3000\}$. Each shape is defined on 5.

For each $S \in \{\text{circle, ellipse, line, parabola, LB, NACA}\}$, we sample 5 independent instances by drawing all shape parameters (centers, radius, semi-axes, vertex offsets, scales, chord lengths, and series codes) uniformly from their prescribed domains. We then choose $n \in \{4\}$ uniformly at random and sample each curve at n equally-spaced parameter values to obtain $\{(x_i, y_i)\}_{i=1}^n$, which serve as the target profiles.

Lemniscate of Bernoulli The lemniscate of Bernoulli is a figure-eight-shaped curve defined by the quartic equation $(x^2 + y^2)^2 = 2a^2(x^2 - y^2)$, where the parameter a controls its overall size. It is symmetric about both axes and consists of two lobes meeting at the origin, exemplifying a simple rational algebraic curve.

NACA Four-Digit Airfoils Each NACA four-digit airfoil is specified by a code (e.g., “2412”) indicating maximum camber, camber position, and thickness relative to chord length. Upper and lower

$$\begin{aligned}
\mathcal{C}(r, x_1, y_1) &= \{(x, y) \mid (x - x_1)^2 + (y - y_1)^2 = r^2\}, \\
\mathcal{E}(a, b, x_1, y_1) &= \{(x, y) \mid \frac{(x - x_1)^2}{a^2} + \frac{(y - y_1)^2}{b^2} = 1\}, \\
\mathcal{L}(x_1, y_1, x_2, y_2) &= \left\{(x, y) \mid y - y_1 = \frac{y_2 - y_1}{x_2 - x_1}(x - x_1)\right\}, \\
\mathcal{P}(a, h, k) &= \{(x, y) \mid y = a(x - h)^2 + k\}, \\
\mathcal{B}(a) &= \{(x, y) \mid (x^2 + y^2)^2 = 2a^2(x^2 - y^2)\}, \\
\mathcal{N}(\text{series}) &= \{(x, y) \mid (x, y) \text{ satisfies the standard NACA upper/lower formulas}\}.
\end{aligned}$$

surface coordinates are generated by piecewise analytic formulas that ensure smooth curvature and typical aerodynamic properties, making them standard in preliminary wing design.

D Reference Metrics

The **Chamfer distance** is a measure of similarity between two point sets P and Q . Intuitively, it sums for each point in P the distance to its nearest neighbor in Q , and vice versa. Formally, one common formulation is 6.

Pass@ measures the end-to-end success rate of a generative system when allowed k independent attempts per problem. Intuitively, it captures the probability that at least one of those k samples “passes” a specified correctness test. In our setting, each candidate program is deemed successful only if it (i) parses without syntax errors and (ii) runs to completion under the target simulator. Formally, Let p be the per-sample success probability, estimated from past runs.

Let

$$k = I \times S$$

be the total number of iterations I times the number of samples per iteration S , and let

$$p = \frac{c}{n}$$

be the observed success ratio (number of successes c over total attempts n). Then

$$\text{Pass}@k = 1 - (1 - p)^k$$

, which directly quantifies the cumulative success over all k iterations.

E Designer Agent ($\mathbb{D}a$) Prompt

14 serves as the template for the $\mathbb{D}a$ Prompt. It provides the structure and context that guides the

$\mathbb{D}a$ in understanding how to approach and execute design of a planar mechanism.

You are an AI specialized in designing planar mechanisms. Based on the description, generate the appropriate mechanism using Python with the `pylinkage` library and explain each component step by step.

Commands (API Documentation): [{api_doc}](#)

Examples:

```
# Example 1
import pylinkage as pl
crank = pl.Crank(x=0, y=0, joint0=(0, 0),
                  distance=1, angle=0.1, name="Crank")
slider = pl.Linear(x=2, y=0,
                   joint0=crank, joint1=(0, 0), joint2=(1, 0),
                   revolute_radius=1.5, name="target")
```

{memory}

The analytical equation describing the motion of the target joint in the above code is given by: {equation} The Chamfer distance of the target equation in the above code is: {score}

Our goal is to minimise the distance. Therefore, the greater the distance, the more it is not following the target motion and deviating from the intended path.

Planar Mechanism Description:

{description}

The mechanism must pass as close as possible through all these points: {points}

Target analytical equation of the motion of the target joint: {target_equation}

Planar Mechanism Code:

$$d_{Chamfer}(P, Q) = \frac{\sum_{p \in P} \min_{q \in Q} \|p - q\|^2}{|P|} + \frac{\sum_{q \in Q} \min_{p \in P} \|q - p\|^2}{|Q|}$$

Legend for Colour Coding:

- **Brown:** Agent Role.
- **Violet:** Chain-of-Thoughts (CoT).
- **Red:** API Documentation and Mechanism Descriptions.
- **Blue:** Examples and code snippets.
- **Cyan:** Memory: previously retained knowledge.
- **Green:** Key points or constraints (e.g., points through which the mechanism must pass).
- **Orange:** Target analytical equation defining ideal behavior.
- **Purple:** Final mechanism code output.

F Critique Agent ($\mathbb{C}a$) Prompt

14 acts as the template for the $\mathbb{C}a$ Prompt. It outlines the format and expectations that help the $\mathbb{C}a$ deliver clear, structured, and constructive critiques to support design improvement and decision-making.

You are a reviewer for a mechanical designer AI agent.

The following planar mechanism description: {description}

Simulator Output: {simulator_output}
{memory}

The analytical equation describing the motion of the target joint in the above code is given by: {equation} The Chamfer distance of the target equation in the above code is: {score}

Our goal is to minimise the distance. Therefore, the greater the distance, the more it is not following the target motion and deviating from the intended path.

The following response was generated to

fulfill the planar mechanism description:

Response: {designer_response}

Your task is to evaluate the correctness, completeness, and complexity of the designed planar mechanism.

Check for consistency with the problem constraints and point out any errors or improvements needed.

Evaluate the complexity of the mechanism design in terms of: Structural Complexity: Assess whether the design is overly complex or can be simplified while maintaining functionality.

Structural Complexity: Assess whether the design is overly complex or can be simplified while maintaining functionality.

Design Elegance: Consider whether the design achieves the required functionality with minimal components or steps, adhering to principles of simplicity and elegance.

Provide feedback in plain text. Point out areas where complexity could be reduced, and suggest improvements if necessary.

Legend for Colour Coding:

- **Brown:** Agent's Role.
- **Red:** Planar mechanism description.
- **Orange:** Simulator output.
- **Cyan:** Memory: previously retained knowledge.
- **Purple:** Designer's response.
- **Teal:** Agent's task.

G Designer Agent ($\mathbb{D}a$) Revision Prompt

15 serves as the template for the $\mathbb{D}a$ Revision Prompt. It provides the structure and context that guides the $\mathbb{D}a$ in understanding how to approach and execute design revisions effectively.

You previously generated the following response for a planar mechanism description: `{designer_response}`

The reviewer provided the following feedback: `{critique_response}`

Simulator Output: `{simulator_output}`
`{memory}`

The analytical equation describing the motion of the target joint in the above code is given by: `{equation}` The Chamfer distance of the target equation in the above code is: `{score}`

Our goal is to minimise the distance. Therefore, the greater the distance, the more it is not following the target motion and deviating from the intended path.

Please revise your response to address the feedback and improve the planar mechanism.

The model should structure the response ensuring each step has only one line of code, ensuring clarity and logical progression, strictly adhering to the commands provided.

Planar Mechanism Code:

Legend for Colour Coding:

- **Purple:** Previously generated response (initial planar mechanism code).
- **Magenta:** Reviewer feedback.
- **Orange:** Simulator output.
- **Cyan:** Memory: previously retained knowledge.
- **Teal:** Agent’s task.

H Shape Complexity

In this section, we present metrics for quantifying shape complexity and compare them to our ground truth and agent-generated forms (Table 2). This concise analysis illustrates how fidelity deteriorates (or remains stable) as geometric intricacy increases. By comparing complexity scores directly across shapes, we can identify the limits of our agent’s performance.

I Qualitative Results

Figures 7,9,11,13,15, and 17, shows the ground-truth targets, while Figures 8, 10,12, 14, 16, and 18 shows the corresponding outputs produced by our agent. Close inspection reveals that many of the generated results closely align with their targets, accurately capturing both the global structure and fine-scale details. This strong visual correspondence highlights the effectiveness of our method in approximating the desired outputs across a range of diverse test cases.

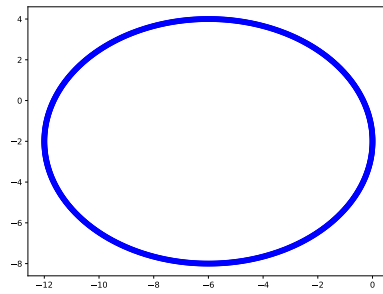


Figure 7: Ground truth Ellipse: the original target Ellipse used for evaluation.

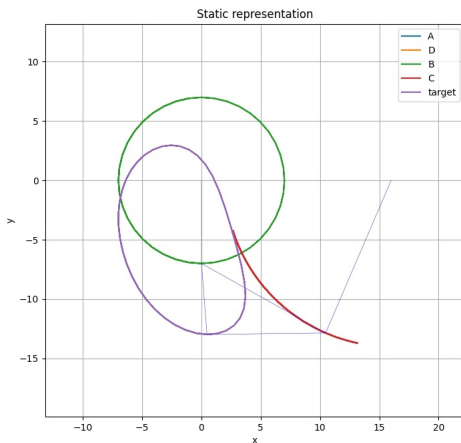


Figure 8: Generated Ellipse: the Ellipse synthesised by our agent.

J Hardware Configuration

We used a workstation equipped with five NVIDIA RTX 3090 graphics cards, each with 24 GB of VRAM and 72 GB of system RAM.

K Extended Quantitative Result

In this section, we present the outcomes of our complete set of experiments, summarising performance

Shape	Mean Chamfer distance
LB	6.4138 ± 2.3978
Circle	7.0547 ± 5.0305
Ellipse	7.8366 ± 3.7530
Line	33.3170 ± 33.7500
Parabola	215.5491 ± 81.2419
NACA	$15725.1416 \pm 13183.1264$

Table 2: The mean Chamfer distances (\pm standard deviation) are shown for each shape category, calculated from the motion of the contours generated by the planar mechanism and the ground-truth contours.

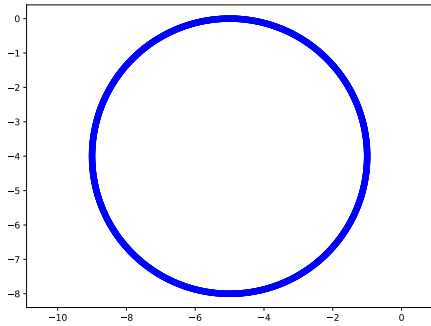


Figure 9: Ground truth Circle: the original target Circle used for evaluation.

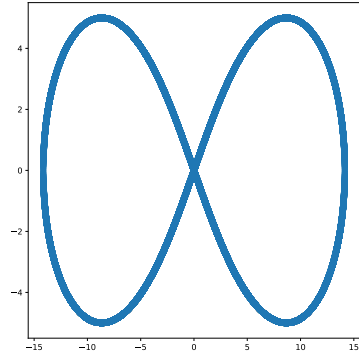


Figure 11: Ground truth LB: the original target LB used for evaluation.

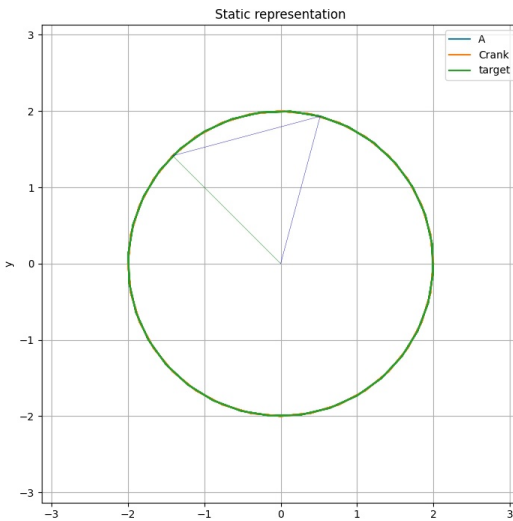


Figure 10: Generated Circle: the Circle synthesised by our agent.

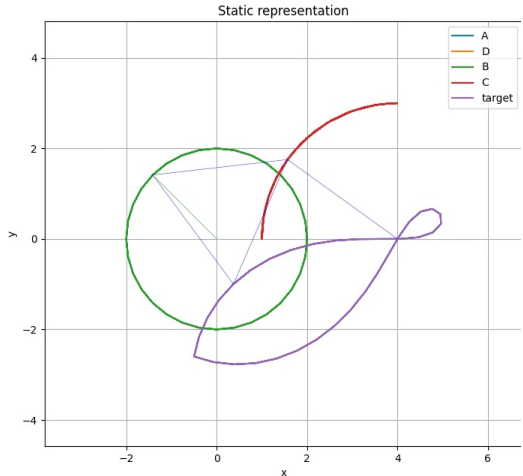


Figure 12: Generated LB: the LB synthesised by our agent.

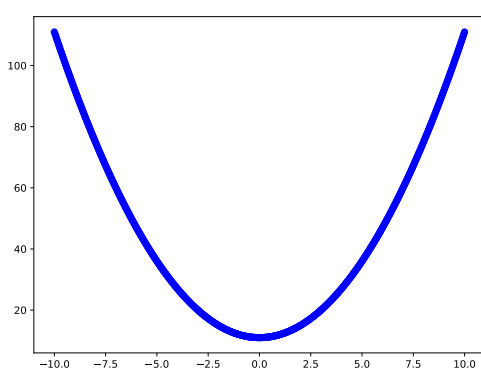


Figure 13: Ground truth Parabola: the original target Parabola used for evaluation.

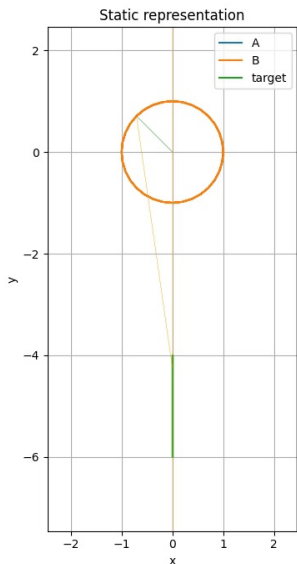


Figure 16: Generated Line: the Line synthesised by our agent.

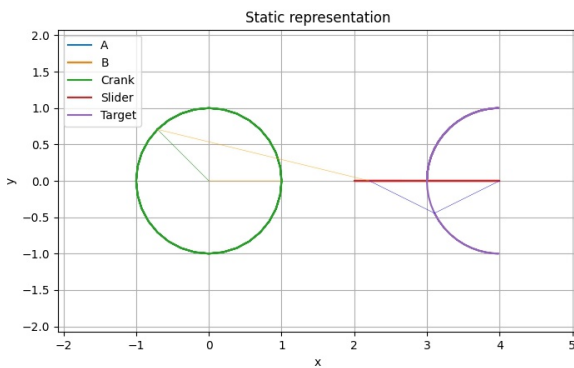


Figure 14: Generated Parabola: the Parabola synthesised by our agent.

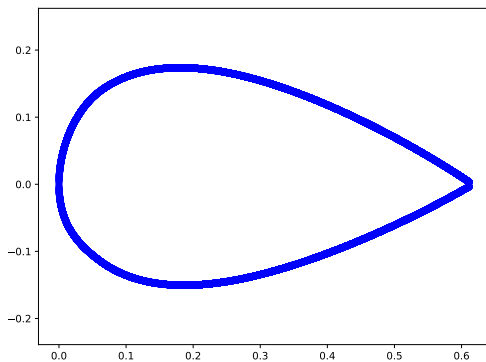


Figure 17: Ground truth NACA airfoil: the original target NACA airfoil used for evaluation.

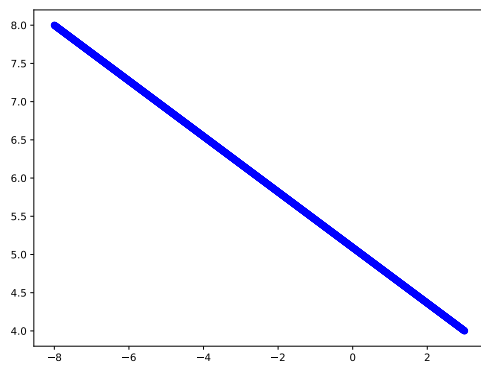


Figure 15: Ground truth Line: the original target Line used for evaluation.

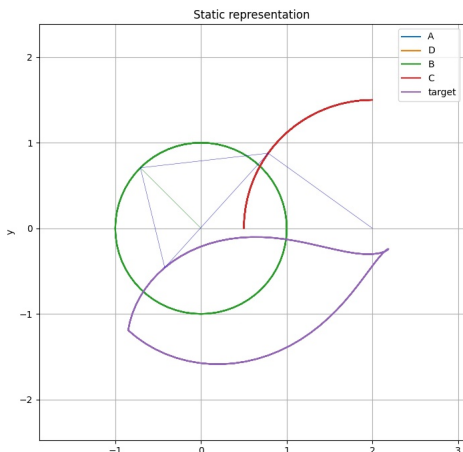


Figure 18: Generated NACA airfoil: the NACA airfoil synthesised by our agent.

across all six shape categories. Table 3 displays quantitative metrics, such as the average Chamfer distance and the number of convergence steps, for agent-generated outputs.

Model	Shape	#Ex	Fdbk	Eqn	Mem	Steps	Best Chamf.	First	First Chamf.	% Imp.	Pass@
gemma3:12b	LB	2	No	No	0	7.5	6.11	2.75	7.905	22.71	0.9845
	LB	2	No	No	2	5	9.01	5	9.01	0.00	0.95308
	LB	2	No	Yes	2	4.25	7.738	4.25	7.978	3.00	0.9191
	LB	2	Yes	No	0	8.25	5.552	1.5	8.081	31.30	1
	LB	2	Yes	No	2	11	6.165	1.75	7.871	21.67	1
	LB	2	Yes	Yes	2	12.25	6.546	2	7.737	15.40	1
	LB	3	No	No	0	7.333	7.991	4	11.47	30.33	0.97931
	LB	3	No	No	2	4	7.778	1.5	8.012	2.92	0.91157
	LB	3	No	Yes	2	8.333	8.439	8.333	8.439	0.00	0.89744
	LB	3	Yes	No	0	10.75	5.917	2	7.857	24.70	1
	LB	3	Yes	No	2	16.25	6.266	2.5	8.088	22.53	1
	LB	3	Yes	Yes	2	12.25	6.29	2.75	6.843	8.08	0.99994
	Circle	2	No	No	0	12.5	14.61	12.5	14.61	0.00	0.91157
	Circle	2	No	No	2	8.5	11.94	8.5	11.94	0.00	0.9346
	Circle	2	No	Yes	2	4	14	4	14	0.00	0.91157
	Circle	2	Yes	No	0	10.8	11.65	5.2	13.68	14.82	0.97203
	Circle	2	Yes	No	2	15	12.19	6	13.32	8.50	1
	Circle	2	Yes	Yes	2	15	13.86	8.2	16.49	15.95	0.99985
	Circle	3	No	No	0	14.25	10.64	6.5	15.51	31.40	0.9346
	Circle	3	No	No	2	5.25	12.99	5.25	14.21	8.59	0.91157
	Circle	3	No	Yes	2	5.75	13.51	5.75	13.51	0.00	0.8692
	Circle	3	Yes	No	0	6	9.449	2.2	13.42	29.57	0.99999
	Circle	3	Yes	No	2	8	12.9	1.4	14	7.81	0.99998
	Circle	3	Yes	Yes	2	10.4	13.7	2.4	16.1	14.89	1
	Ellipse	2	No	No	0	5	11.41	5	11.41	0.00	0.8692
	Ellipse	2	No	No	2	7	11.53	7	11.53	0.00	0.8943
	Ellipse	2	No	Yes	2	14	10	14	10	0.00	0.8692
	Ellipse	2	Yes	No	0	9.333	8.607	7.667	9.354	7.98	0.93765
	Ellipse	2	Yes	No	2	10.75	9.019	7.5	15.54	41.95	0.99947
	Ellipse	2	Yes	Yes	2	13	9.366	4.333	10.49	10.76	0.99999
	Ellipse	3	No	No	0	13	8.884	13	8.884	0.00	0.95393
	Ellipse	3	No	No	2	6.5	10.2	6.5	10.2	0.00	0.91157
	Ellipse	3	No	Yes	2	12	10.34	12	10.34	0.00	0.8692
	Ellipse	3	Yes	No	0	8	9.868	8	11.29	12.62	0.95811
	Ellipse	3	Yes	No	2	12.33	8.383	9.333	8.459	0.89	0.95561
	Ellipse	3	Yes	Yes	2	15.5	11.74	10	11.93	1.60	0.93195
	Line	2	No	No	0	11	38.99	8.75	39.75	1.91	0.94412
	Line	2	No	No	2	9	50.01	9	50.01	0.00	0.94104
	Line	2	No	Yes	2	9.667	23.75	9.667	23.75	0.00	0.89744
	Line	2	Yes	No	0	9.8	36.36	7	38.37	5.23	0.9686
	Line	2	Yes	No	2	10.8	36.46	3	38.52	5.37	1
	Line	2	Yes	Yes	2	14.8	37.53	2.2	39.51	5.01	0.99879
	Line	3	No	No	0	10.4	39.7	5.2	41.16	3.55	0.96957
	Line	3	No	No	2	1.5	47.09	1.5	47.09	0.00	0.89038
	Line	3	No	Yes	2	4.25	43.86	4.25	43.86	0.00	0.90055
	Line	3	Yes	No	0	10.8	37.71	4.4	40.2	6.19	0.97296
	Line	3	Yes	No	2	10	37.14	3.2	38.84	4.38	0.99995
	Line	3	Yes	Yes	2	7	38.33	2.6	40.17	4.60	0.98699

Model	Shape	#Ex	Fdbk	Eqn	Mem	Steps	Best Chamf.	First	First Chamf.	% Imp.	Pass@
gemma3:12b	NACA	2	No	No	0	2.2	1.573e+04	1.2	1.573e+04	0.00	1
	NACA	2	No	No	2	1.8	1.573e+04	1.6	1.573e+04	0.00	0.97201
	NACA	2	No	Yes	2	1.2	1.573e+04	1.2	1.573e+04	0.00	0.94131
	NACA	2	Yes	No	0	10.6	1.573e+04	1.2	1.573e+04	0.00	1
	NACA	2	Yes	No	2	11.2	1.573e+04	1.8	1.573e+04	0.00	0.99998
	NACA	2	Yes	Yes	2	8.8	1.572e+04	1.8	1.573e+04	0.00	0.99998
	NACA	3	No	No	0	2.4	1.573e+04	1.4	1.573e+04	0.00	0.99985
	NACA	3	No	No	2	3	1.573e+04	2	1.573e+04	0.00	0.92004
	NACA	3	No	Yes	2	3	1.573e+04	3	1.573e+04	0.00	0.93209
	NACA	3	Yes	No	0	3.8	1.573e+04	1.4	1.573e+04	0.01	1
	NACA	3	Yes	No	2	6	1.573e+04	1.8	1.573e+04	0.00	0.98984
	NACA	3	Yes	Yes	2	3.8	1.573e+04	1.6	1.573e+04	0.00	0.99879
	Parabola	2	No	No	0	14.67	158.2	9	163.5	3.25	0.95628
	Parabola	2	No	No	2	5.75	208.3	5.75	208.3	0.00	0.98847

Model	Shape	#Ex	Fdbk	Eqn	Mem	Steps	Best	Chamf.	First	First Chamf.	% Imp.	Pass@
llama3.3:70b	LB	2	No	No	0	7.75	4.615	2.5	10.01	53.90	0.99999	
	LB	2	No	No	2	6.75	5.426	1.75	6.73	19.37	1	
	LB	2	No	Yes	2	5.75	5.229	2.5	6.661	21.50	1	
	LB	2	Yes	No	0	9	5.34	1.75	10.77	50.44	0.99999	
	LB	2	Yes	No	2	15	5.491	1.25	9.972	44.94	1	
	LB	2	Yes	Yes	2	12.33	5.174	2.667	6.803	23.95	1	
	LB	3	No	No	0	4.75	4.976	1.25	7.706	35.43	1	
	LB	3	No	No	2	9.25	6.292	1.75	7.739	18.69	1	
	LB	3	No	Yes	2	8.75	8.195	1	13.6	39.74	1	
	LB	3	Yes	No	0	8.25	5.304	1.25	9.716	45.41	1	
	LB	3	Yes	No	2	14.5	5.252	1.75	8.676	39.46	1	
	LB	3	Yes	Yes	2	8	10.27	2	12.74	19.38	1	
	Circle	2	No	No	0	10.4	4.587	4.2	9.825	53.31	0.99916	
	Circle	2	No	No	2	7.6	9.536	1.6	9.883	3.51	1	
	Circle	2	No	Yes	2	8.6	4.074	2.6	8.347	51.19	1	
	Circle	2	Yes	No	0	7.8	2.86	1.6	13.53	78.87	1	
	Circle	2	Yes	No	2	13.2	3.911	1.4	12.42	68.52	1	
	Circle	2	Yes	Yes	2	12.2	5.37	4.4	6.762	20.58	0.99985	
	Circle	3	No	No	0	6.4	3.588	1.6	7.998	55.14	0.99996	
	Circle	3	No	No	2	11.2	7.541	2	12.71	40.65	1	
	Circle	3	No	Yes	2	8	7.651	3.8	10.63	28.03	1	
	Circle	3	Yes	No	0	7.6	3.377	2	10.54	67.95	0.99999	
	Circle	3	Yes	No	2	12.8	3.833	1.4	10.82	64.57	1	
	Circle	3	Yes	Yes	2	10.2	6.437	1.4	12.41	48.13	1	
	Ellipse	2	No	No	0	11.75	5.088	2.5	10.01	49.15	1	
	Ellipse	2	No	No	2	5	6.83	1	10.49	34.88	1	
	Ellipse	2	No	Yes	2	12.25	5.909	3.5	9.103	35.08	0.99602	
	Ellipse	2	Yes	No	0	7.5	5.167	1	10.53	50.94	1	
	Ellipse	2	Yes	No	2	11.25	5.275	1	11.3	53.30	1	
	Ellipse	2	Yes	Yes	2	12	6.514	1.75	10.39	37.31	1	
	Ellipse	3	No	No	0	10.5	4.937	1.25	10.2	51.57	0.99995	
	Ellipse	3	No	No	2	9.75	8.946	1.75	9.773	8.47	1	
	Ellipse	3	No	Yes	2	9.5	12.5	3.25	16.14	22.58	1	
	Ellipse	3	Yes	No	0	7.5	4.771	1	10.42	54.20	1	
	Ellipse	3	Yes	No	2	16.25	6.606	1.25	13.8	52.11	1	
	Ellipse	3	Yes	Yes	2	9.75	5.252	2.25	8.681	39.50	1	
	Line	2	No	No	0	11	27.6	2.2	35.97	23.26	0.99947	
	Line	2	No	No	2	8.2	37.05	3	37.66	1.62	1	
	Line	2	No	Yes	2	8.2	33.09	4	34.15	3.10	1	
	Line	2	Yes	No	0	5.2	31.27	1.6	36.92	15.29	1	
	Line	2	Yes	No	2	12	29.52	1	37.57	21.43	1	
	Line	2	Yes	Yes	2	13	30.48	2.4	38.82	21.48	1	
	Line	3	No	No	0	10.2	27.97	2.4	30.53	8.39	0.99998	
	Line	3	No	No	2	4	32.66	2.4	32.73	0.23	1	
	Line	3	No	Yes	2	11.4	35.66	1.6	37.36	4.54	0.99988	
	Line	3	Yes	No	0	12	29.8	1.8	37.46	20.44	1	
	Line	3	Yes	No	2	15.2	26.15	1.2	39.77	34.25	1	
	Line	3	Yes	Yes	2	9.6	34.36	2.8	35.53	3.28	0.99999	

Model	Shape	#Ex	Fdbk	Eqn	Mem	Steps	Best Chamf.	First	First Chamf.	% Imp.	Pass@
Ilama3.3:70b	NACA	2	No	No	0	10.4	1.572e+04	2.6	1.573e+04	0.00	0.99964
	NACA	2	No	No	2	10.2	1.573e+04	2.6	1.573e+04	0.00	1
	NACA	2	No	Yes	2	9.8	1.573e+04	2.2	1.573e+04	0.00	1
	NACA	2	Yes	No	0	4	1.572e+04	2	1.573e+04	0.00	0.99983
	NACA	2	Yes	No	2	12.8	1.573e+04	1.8	1.573e+04	0.00	0.99999
	NACA	2	Yes	Yes	2	10.6	1.572e+04	4.6	1.573e+04	0.00	1
	NACA	3	No	No	0	8.6	1.572e+04	1.2	1.573e+04	0.00	0.99999
	NACA	3	No	No	2	7.6	1.572e+04	2.6	1.573e+04	0.00	1
	NACA	3	No	Yes	2	7	1.573e+04	1.8	1.573e+04	0.00	1
	NACA	3	Yes	No	0	8.4	1.572e+04	1.6	1.573e+04	0.00	0.99982
	NACA	3	Yes	No	2	10.8	1.572e+04	2.8	1.573e+04	0.00	1
	NACA	3	Yes	Yes	2	8.2	1.573e+04	2.6	1.573e+04	0.00	1
	Parabola	2	No	No	0	14.2	199.1	2	235.1	15.31	1
	Parabola	2	No	No	2	7.8	215.8	1	222.6	3.06	1
	Parabola	2	No	Yes	2	11	217.1	1.8	221.2	1.85	1
	Parabola	2	Yes	No	0	6.4	189	1.4	226	16.38	0.99955
	Parabola	2	Yes	No	2	12.4	199.5	1.6	220.6	9.53	1
	Parabola	2	Yes	Yes	2	14.2	215.4	1.2	226.7	4.96	1
	Parabola	3	No	No	0	12.4	188.5	2	221.4	14.85	1
	Parabola	3	No	No	2	8.4	225	1.6	235.1	4.30	1
	Parabola	3	No	Yes	2	5.4	205.3	1.4	223.1	8.01	0.99964
	Parabola	3	Yes	No	0	9.4	195.9	1.2	230.2	14.90	0.99943
	Parabola	3	Yes	No	2	10.8	215.6	1.6	229.7	6.14	1
	Parabola	3	Yes	Yes	2	13	199.9	1	221.1	9.58	1

Model	Shape	#Ex	Fdbk	Eqn	Mem	Steps	Best Chamf.	First	First Chamf.	% Imp.	Pass@
qwen3:4b	LB	2	No	No	0	8.5	6.163	1	8.953	31.16	1
	LB	2	No	No	2	9.25	6.807	3.25	6.807	0.00	0.97298
	LB	2	No	Yes	2	5.167	7.994	2.167	9.709	17.67	0.9778
	LB	2	Yes	No	0	7.333	6.23	1	10.46	40.44	1
	LB	2	Yes	No	2	11	5.762	1.75	9.985	42.30	1
	LB	2	Yes	Yes	2	6.8	7.198	2	8.401	14.33	1
	LB	3	No	No	0	7.8	5.708	1.6	6.828	16.41	0.99959
	LB	3	No	No	2	13.8	6.722	1.6	7.762	13.40	0.99988
	LB	3	No	Yes	2	9.5	6.636	2.75	6.935	4.31	0.9973
	LB	3	Yes	No	0	15.25	5.701	2.25	7.215	20.98	1
	LB	3	Yes	No	2	11.6	5.886	1.8	6.683	11.94	1
	LB	3	Yes	Yes	2	8.5	6.3	1.75	6.924	9.02	1
	Circle	2	No	No	0	10.6	5.26	4.2	6	12.33	0.99079
	Circle	2	No	No	2	6.2	3.732	3.2	6	37.79	1
	Circle	2	No	Yes	2	8.2	5.739	5	7.315	21.54	0.99067
	Circle	2	Yes	No	0	4	5.432	2.75	6	9.47	0.99545
	Circle	2	Yes	No	2	7	3.783	4.6	6	36.94	0.99642
	Circle	2	Yes	Yes	2	8.2	3.881	3.8	6	35.31	1
	Circle	3	No	No	0	10	4.737	3.6	6	21.06	0.99065
	Circle	3	No	No	2	6.4	3.748	3.8	4.427	15.32	1
	Circle	3	No	Yes	2	9.2	3.692	1.8	6	38.46	1
	Circle	3	Yes	No	0	2.8	5.467	2.6	5.68	3.75	0.9661
	Circle	3	Yes	No	2	10	3.815	7.8	5.467	30.22	0.99628
	Circle	3	Yes	Yes	2	11.25	4.463	6.75	5.805	23.12	0.99572
	Ellipse	2	No	No	0	9	4.965	2.5	11.17	55.56	0.99896
	Ellipse	2	No	No	2	3.667	9.631	2	10.04	4.02	0.99998
	Ellipse	2	No	Yes	2	12.5	8.384	3.75	9.254	9.41	0.9995
	Ellipse	2	Yes	No	0	10.75	5.991	5.25	8.508	29.59	0.96665
	Ellipse	2	Yes	No	2	4.333	6.662	1	10.71	37.80	1
	Ellipse	2	Yes	Yes	2	5.25	9.902	1.5	13.16	24.76	1
	Ellipse	3	No	No	0	10.75	5.903	2.75	12.17	51.49	0.98848
	Ellipse	3	No	No	2	5.25	11.19	1.5	16.15	30.67	0.99966
	Ellipse	3	No	Yes	2	8	9.936	3	17.66	43.75	0.9998
	Ellipse	3	Yes	No	0	9.5	8.826	1.5	11.03	20.00	0.99847
	Ellipse	3	Yes	No	2	10	9.883	2.75	13.48	26.68	0.98802
	Ellipse	3	Yes	Yes	2	9.25	6.391	1.25	12.05	46.97	0.99999
	Line	2	No	No	0	7.6	32.51	5.8	32.73	0.68	0.96024
	Line	2	No	No	2	6.2	31.45	2.4	31.66	0.67	1
	Line	2	No	Yes	2	8.2	34.57	5.8	34.57	0.01	0.99916
	Line	2	Yes	No	0	10.4	28.28	3.8	35.69	20.76	0.99835
	Line	2	Yes	No	2	5.4	32.58	2.8	34.83	6.44	1
	Line	2	Yes	Yes	2	11.6	32.86	2.6	36.1	8.97	0.99879
	Line	3	No	No	0	10.6	28.7	6	29.07	1.25	0.96461
	Line	3	No	No	2	6.75	15.52	3.75	17.2	9.77	0.99955
	Line	3	No	Yes	2	6	33.42	4	34.34	2.70	0.98759
	Line	3	Yes	No	0	7.4	30.63	4	31.45	2.59	0.99007
	Line	3	Yes	No	2	7.2	29.73	3.4	45.54	34.72	0.99012
	Line	3	Yes	Yes	2	11	31.92	8	32.04	0.38	0.99637

Model	Shape	#Ex	Fdbk	Eqn	Mem	Steps	Best Chamf.	First	First Chamf.	% Imp.	Pass@
qwen3:4b	NACA	2	No	No	0	4.4	1.572e+04	1.2	1.573e+04	0.01	1
	NACA	2	No	No	2	12.8	1.573e+04	1.2	1.573e+04	0.00	0.99999
	NACA	2	No	Yes	2	5.4	1.573e+04	1	1.573e+04	0.00	1
	NACA	2	Yes	No	0	7.6	1.573e+04	1	1.573e+04	0.01	1
	NACA	2	Yes	No	2	10.8	1.573e+04	1.2	1.573e+04	0.00	0.99999
	NACA	2	Yes	Yes	2	8.8	1.573e+04	1	1.573e+04	0.01	0.99958
	NACA	3	No	No	0	5.4	1.573e+04	1.4	1.573e+04	0.00	1
	NACA	3	No	No	2	10	1.573e+04	1.4	1.573e+04	0.00	0.99665
	NACA	3	No	Yes	2	7	1.573e+04	1.2	1.573e+04	0.00	0.99988
	NACA	3	Yes	No	0	8.2	1.572e+04	1	1.573e+04	0.00	1
	NACA	3	Yes	No	2	10.4	1.572e+04	1.4	1.573e+04	0.00	0.99957
	NACA	3	Yes	Yes	2	11.4	1.573e+04	1.2	1.573e+04	0.00	0.99999
	Parabola	2	No	No	0	10.8	216.4	1.4	235	7.91	1
	Parabola	2	No	No	2	18	208.7	1	235.6	11.40	1
	Parabola	2	No	Yes	2	15.2	213	1	233.7	8.83	1

Table 3: Performance results across shapes and settings